Journal Pre-proof

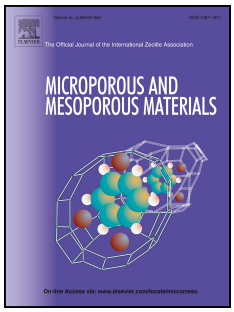

Facile synthesis of dual-functionalized microporous organic network for efficient removal of cationic dyes from water

Xue Li, Yuan-Yuan Cui, Ying-Jun Chen, Cheng-Xiong Yang, Xiu-Ping Yan

PII: S1387-1811(20)30016-0

DOI: https://doi.org/10.1016/j.micromeso.2020.110013

Reference: MICMAT 110013

To appear in: *Microporous and Mesoporous Materials*

Received Date: 9 October 2019

Revised Date: 31 December 2019

Accepted Date: 6 January 2020

Please cite this article as: X. Li, Y.-Y. Cui, Y.-J. Chen, C.-X. Yang, X.-P. Yan, Facile synthesis of dual-functionalized microporous organic network for efficient removal of cationic dyes from water, *Microporous and Mesoporous Materials* (2020), doi: https://doi.org/10.1016/j.micromeso.2020.110013.

Graphical Abstract

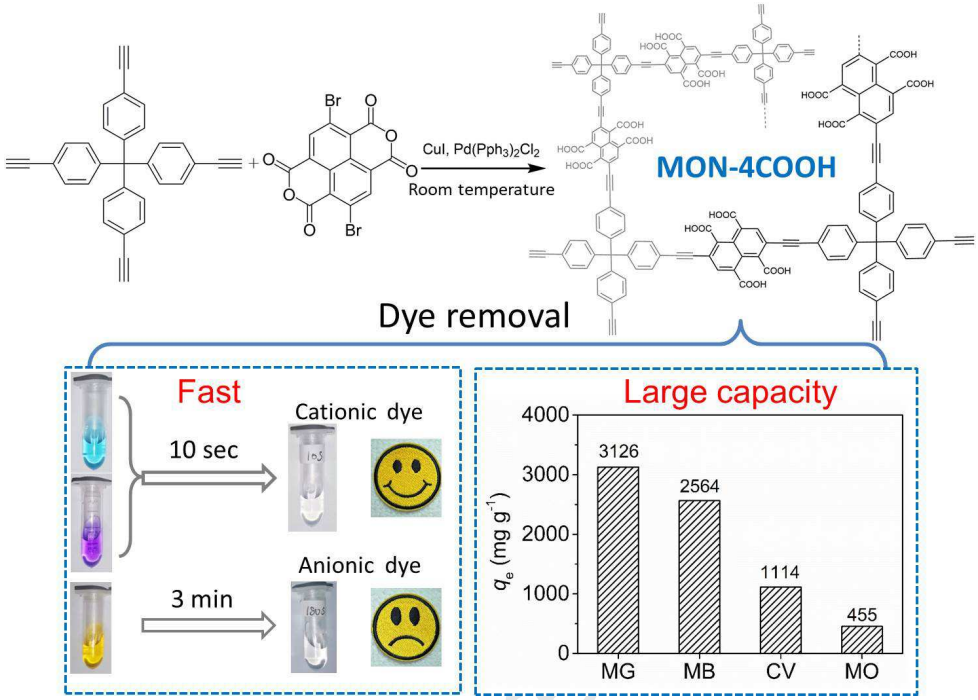

Facile synthesis of dual-functionalized microporous organic network for efficient removal of cationic dyes from water

Xue Li[b], Yuan-Yuan Cui[a], Ying-Jun Chen[a], Cheng-Xiong Yang[a,*], Xiu-Ping Yan[c]

[a] *College of Chemistry, Research Center for Analytical Sciences, Tianjin Key Laboratory of Molecular Recognition and Biosensing, Nankai University, Tianjin 300071, China*

[b] *Tianjin State Key Laboratory of Modern Chinese Medicine & Tianjin Key Laboratory of TCM Chemistry and Analysis, Tianjin University of Traditional Chinese Medicine, Tianjin 300193, China*

[c] *State Key Laboratory of Food Science and Technology, International Joint Laboratory on Food Safety, Institute of Analytical Food Safety, School of Food Science and Technology, Jiangnan University, Wuxi 214122, China*

*Corresponding author.

E-mail: cxyang@nankai.edu.cn

ABSTRACT

A facile one-step anhydride hydrolysis strategy was rationally designed to synthesize a novel dual-functionalized microporous organic network (MON-4COOH) with enriched naphthalene and carboxyl groups for efficient removal of cationic dyes. The pre-designed electrostatic, hydrogen bonding, π-π and hydrophobic interaction sites on MON-4COOH led to the complete removal of three typical cationic dyes methylene blue, malachite green and crystal violet (25 mg L^{-1} for each) within 20 seconds and gave their maximum adsorption capacities of 2564, 3126 and 1114 mg g^{-1}, respectively. The adsorption of these cationic dyes fitted well with pseudo-second-order kinetic and Langmuir adsorption models. The adsorption kinetics and capacities of these cationic dyes on MON-4COOH were much faster and higher than many other reported adsorbents. The negatively charged MON-4COOH also gave much faster adsorption kinetic and larger adsorption capacity for cationic (methylene blue, malachite green and crystal violet) dyes than anionic dye. The excellent flow-through water treatment ability and reusability also made MON-4COOH highly potential for the remediation of cationic dyes polluted water. This work provided a feasible way to design and synthesize of dual-functionalized MONs for efficient adsorption and elimination of environmental pollutants from water.

Keywords:

Microporous organic network; Dual-functionalized; Adsorption; Removal; Cationic dyes;

1. Introduction

Water pollution has received increase attention due to the safety and scarcity of drinking water [1,2]. According to the World Bank report, the water-soluble organic dyes are considered to be the main contributors in water contamination [3]. The abuse and illegal discharge of organic dyes have caused serious environmental pollution and threat for human beings and aquatic life because the organic dyes are usually highly toxic, mutagenic, carcinogenic and hard to biodegrade [4-6]. Therefore, development of efficient and convenient methods for the removal and elimination of organic dyes from water are of extremely significant for environmental protection and drinking water safety [7-9].

The adsorption has been proven to be an attractive strategy for the elimination of organic dyes from water because of its high efficiency and simplicity [10]. The adsorbents play the dominant roles either for the selectivity or for the efficiency during the adsorption of organic dyes. The rational design and synthesis of efficient adsorbents to remove organic dyes from water have become an emergent and challenging topic. Until now, porous materials such as carbon nanotubes [11], layered double hydroxide [12], yolk-shell magnetic porous organic nanospheres [13], lignocellulose gels [14], magnetic grapheme oxide [15], polydopamine nanoparticles [16], metal-organic frameworks (MOFs) [17-20], covalent-organic framework [21], MWCNT/alumina composite [22] and silsesquioxane-based hybrid porous polymers [23-26] have been explored as advanced sorbents for efficient adsorption and removal of organic dyes. Development of novel adsorbents with large adsorption capacity and

fast adsorption kinetics is still quite desirable for the removal and elimination of organic dyes from water.

Microporous organic networks (MONs), constructed via the Sonogashira coupling of alkynes and arylhalides, are a recent class of functional porous materials [27-29]. The good solvent and thermal stabilities, large surface area, designable structures and easy loading on other matrix made MONs potential in diverse areas and as advanced adsorbents for the efficient adsorption and removal of hazardous pollutants from water [30-34]. Aromatic benzene rings and ionic functional groups are usually included in organic dyes' structures [4-6]. The π-π, hydrophobic, hydrogen bonding, metal coordination and electrostatic interactions are the possible adsorption mechanisms for the adsorption and removal of organic dyes from water [12-26]. Taking some of these factors into account when designing or modifying the adsorbents would largely improve their removal efficiency for organic dyes.

MONs with conjugate networks may possess good hydrophobic and π-π interactions for organic dyes [35]. Incorporation of hydrogen bonding sites or ionic function groups within MONs' networks would be a feasible way to improve their removal efficiency for organic dyes or hazardous pollutants [36-38]. For example, Liu *et al* reported the post-synthesis of a pyrimidine modified MONs for improving the adsorption efficiency of anionic dyes from water [36]. Our group also showed the fabrication of hydroxyl and amino functionalized MONs for enhancing their removal efficiency for tetrabromobisphenol A [37,38]. The carboxyl groups were served as prior binding sites or groups to cationic dyes [19,20]. The carboxyl-containing porous

materials such as MOFs and resins have been explored for the efficient adsorption and removal of cationic dyes [19,20,39]. Therefore, introduction of carboxyl groups along with hydrophobic sites into MONs' networks may largely enhance their adsorption kinetic and removal efficiency for cationic organic dyes. However, the synthesis of carboxyl enriched MONs for cationic dyes removal has not been reported so far, not to mention the fabrication and application of dual-functionalized MONs for cationic dyes. Anhydride hydrolysis is a typical and commonly used reaction to prepare target acid or carboxyl functionalized materials.

Herein, we report the facile synthesis of a novel dual-functionalized MON (MON-4COOH) for efficient removal of cationic dyes from water (Fig. 1). The naphthalene-contained and carboxyl-enriched MON-4COOH was easily synthesized using 2,6-dibromonaphthalene-1,4,5,8-tetracarboxylic dianhydride (DBTD) as the starting monomer. The anhydride groups within the DBTD can be hydrolyzed to provide multi-carboxyl groups within MON-4COOH under the basic synthesis condition to enhance the adsorption kinetics and removal efficiency for cationic dyes via electrostatic attraction and hydrogen bonding interaction. In addition, the naphthylene groups on networks can further enhance the π-π and hydrophobic interactions of MON-4COOH to the aromatic organic dyes. Based on the above predesigned interaction sites within the networks, the MON-4COOH gave fast adsorption kinetics and large adsorption capacities for three model cationic dyes methylene blue (MB), malachite green (MG) and crystal violet (CV), underling the great potential of MON-4COOH for the removal of cationic dyes and environmental

105 pollutants from water.

106 **2. Materials and methods**

107 *2.1. Chemicals and reagents*

108 All chemicals and reagents used were at least of analytical grade.
109 Bis(triphenylphosphine) palladium dichloride ($Pd(Pph_3)_2Cl_2$, 98%), DBTD (98%) and
110 2,6-dibromonaphthalene (98%) were obtained from TCI Co., Ltd. (Shanghai, China).
111 Tetrakis(4-ethynylphenyl)methane (97%) was bought from Tongchuangyuan
112 Pharmaceutical Technology Co. (Chengdu, China). Copper(I) iodide (CuI, 99.5%)
113 was supplied by Aladdin Chemistry Co., Ltd. (Shanghai, China). Methylene blue (MB,
114 80%), malachite green (MG, 98%), crystal violet (CV, 98%), acid brown 75 (AB75,
115 98%), alizarin red (AR, 85%) and methyl orange (MO, 96%) were purchased from
116 Heowns Biochemical Technology Co., Ltd. (Tianjin, China). HCl (ω, 36%), NaOH
117 (98%), NaCl (95%) and toluene (98%) were obtained from Guangfu Co., Ltd. (Tianjin,
118 China). The ultrapure water was bought from Wahaha Foods Co., Ltd. (Hangzhou,
119 China). Ethanol (99.7%), methanol (99.9%), acetonitrile (99.7%), dichloromethane
120 (99.5%), and triethylamine (99.5%) were purchased from Concord Co., Ltd. (Tianjin,
121 China).

122 *2.2. One-step preparation of MON-4COOH*

123 Typically, CuI (8.8 mg), $Pd(Pph_3)_2Cl_2$ (33.6 mg), toluene (30 mL) and
124 triethylamine (30 mL) were placed in a 100 mL flask. After dissolving under
125 ultrasonicating, DBTD (409 mg, 0.96 mmol) and tetrakis(4-ethynylphenyl)methane
126 (200 mg, 0.48 mmol) were added. The suspension was magnetic stirred at room

temperature for 4 h to synthesize MON-4COOH. The pale brown powder was collected under centrifugation (8000 rpm, 5 min). The collected precipitate was thoroughly washed with dichloromethane and ethanol, and dried under vacuum overnight. The MON-NAP (a control MON without dianhydride groups) was prepared under the same procedures by using 2,6-dibromonaphthalene (275 mg, 0.96 mmol) as the monomer. The MON, MON-COOH, and MON-2COOH were synthesized according to our reported methods [35,37].

2.3. Characterization of MON-4COOH

The synthesized MON-4COOH was characterized with elemental analysis, solid ^{13}C nuclear magnetic resonance (^{13}C NMR), thermogravimetric analysis (TGA), fourier transform infrared (FT-IR), Raman spectroscopy, N_2 adsorption-desorption experiments, field emission scanning electron microscope (FE-SEM), water contact angle and Zeta potential evaluations. Elemental analysis was measured on vario EL CUBE analyzer (Elementar, Germany). The solid ^{13}C-NMR data were measured on Infinityplus 300 (VARIAN, USA). The Raman spectrum was collected on laser confocal Raman spectrometer (InVia Reflex, UK). The TGA curve was recorded on PTC-10A analyzer (Rigaku, Japan). The FT-IR data were recorded on Nicolet AVATAR-360 (Nicolet, USA). N_2 adsorption-desorption isotherms were recorded on ASAP 2010 micropore physisorption analyzer (Micromeritics, Nor-cross, GA, USA). The FE-SEM images were measured on Apreo LoVac (FEI, Czech). The water contact angle was tested on OCA150pro (Beijing, China). The Zeta potentials were performed on a Zetasizer Nano-ZS (Malvern, U.K.). The UV spectra were recorded on UV-3600

spectrophotometer (SHIMADZU, Japan). The X-ray photoelectron spectroscopy (XPS) was measured on Axis Ultra DLD (Kratos, Britain).

2.4. Adsorption experiments

The stock solution of three cationic dyes MB, MG, and CV (10000 mg L^{-1} for each), and an anionic dye MO (2000 mg L^{-1}) were prepared by dissolving proper amount of dyes with ultrapure water. The stock solution was stepwise diluted with ultrapure water to prepare the working solution of each dye.

The adsorption kinetics of four dyes on MON-4COOH were evaluated by dispersing 10 mg of MON-4COOH in 20 mL of target dye solution (initial concentrations of 25, 50 or 100 mg L^{-1}) under vortex shaking. After adsorption for a pre-determined time (0-5 min for MG, MB and CV, and 0-120 min for MO) at room temperature, 1 mL of each solution was collected, filtered with 0.22 μm filter membrane, and measured with UV. Based on the concentrations of target dye before and after adsorption, the adsorption capacity (q_t, mg g^{-1}) at time t (s or min) can be calculated for the kinetics study based on the pseudo-second-order kinetic model (1) [35]:

$$\frac{t}{q_t} = \frac{1}{k_2 q_e^2} + \frac{1}{q_e} t \qquad (1)$$

where k_2 (g mg^{-1} min^{-1}) is the pseudo-second-order rate constant, q_e (mg g^{-1}) is the adsorption capacity at equilibrium.

The adsorption isotherms were studied at the temperature range of 25-55 ^oC. Ten microgram of MON-4COOH was dispersed with 20 mL of the target dye solution. After maintaining at the specified temperature for 2 h, the suspention was filtered with

0.22 μm filter membrane and determined by UV. The Langmuir adsorption model was fitted according to equation (2) [37]:

$$\frac{c_e}{q_e} = \frac{1}{bq_o} + \frac{c_e}{q_o} \qquad (2)$$

where C_e (mg L^{-1}) is the equilibrium concentration of target dye. q_o (mg g^{-1}) is the maximum adsorption capacity. The b (L mg^{-1}) is a constant of the Langmuir adsorption model.

Ten microgram of MON-4COOH was mixed with 20 mL of dye solution at diverse pH (3.0-10.0) or NaCl concentrations (0-50.0 mg L^{-1}). After contacting for 2 h, the suspention was filtered and then measured with UV to explore their effects on adsorption.

2.5. Dye polluted water sample treatment

The solid phase extraction columns were fabicated to study practical use of MON-4COOH for dye polluted water samples. Briefly, 50 mg of MON-4COOH was loaded in a 3 mL empty solid phase extraction column (Thermo Scientific, USA) with both frits fixed. The dye polluted water sample (25 mg L^{-1}) was then separately passed through the column at a flow rate of 2.0 mL min^{-1} with the aid of a FIA-3100 flow injection analyzer (Beijing, China). The filtrate was then collected for UV analysis.

3. Results and discussion

3.1. Characterization

The elemental analysis, solid ^{13}C NMR, TGA, FT-IR, Raman spectrum, N_2 adsorption-desorption experiments, FE-SEM, Zeta potential and water contact angle

evaluations were used to characterize the obtained MON-4COOH (Fig. 2; Fig. S1-S2 and Table S1). The chemical shifts of solid ^{13}C NMR at 120-150, and 60-95 ppm were ascribed to the signals of benzyl carbon, aromatic ring and internal alkyne on MON-4COOH, respectively (Fig. 2a) [35]. The chemical shift at 150-170 ppm was assigned to the characteristic peak of carboxyl groups. The FT-IR data revealed the typical -OH and C=O peaks for carboxyl groups at about 3400 and 1700 cm^{-1}, respectively (Fig. 2b) [40]. The characteristic stretching vibration of -C≡C-H and -C≡C- were located at 3200 and 2250 cm^{-1}, respectively. The FT-IR peaks at 1500 and 800 cm^{-1} were assigned to the stretching and bending vibration of aromatic rings on MON-4COOH. In addition, the peak at 3010 cm^{-1} was ascribed to the stretching vibration of C-H of aromatic rings. Raman spectrum also showed the typical characteristic peaks of -OH (3400 cm^{-1}), C=O (1440 cm^{-1}), C≡C (2450 cm^{-1}) and C=C (1525 cm^{-1}) for MON-4COOH [41] (Fig. S2). The elemental analysis revealed the O content of MON-4COOH was much higher than that of MON-NAP without dianhydride groups (Fig. S3-S4; Table S1). These results showed the successful synthesis of carboxyl-enriched MON-4COOH. The N_2 adsorption-desorption isotherms showed the Brunauer-Emmett-Teller (BET) surface area of the MON-4COOH was 847 m^2 g^{-1} (Fig. 2c). The pore size of MON-4COOH was about 1.4 nm (Fig. S5). The TGA curve showed that the MON-4COOH was stable up to 320 ^oC (Fig. 2d). The FE-SEM image revealed the spherical morphology of MON-4COOH with the size of about 400 nm (Fig. 2e). The MON-4COOH gave the water contact angle of 78^o (Fig. 2f), which was much lower than that of MON-NAP

213 (145^{o}; Fig. S4d), revealing the introduction of carboxyl groups onto MON-NAP'
214 networks can largely improve its hydrophilicity. The Zeta potential of MON-4COOH
215 was -55.1 mV at pH=7, which was much lower than that of MON-NAP (-3.8 mV, Fig.
216 S1). All these results revealed the facile and feasible anhydride hydrolysis strategy to
217 synthesize carboxyl-enriched MON-4COOH. As all the four alkynyl groups on
218 tetrakis(4-ethynylphenyl)methane can possibly couple to the Br atoms on DBTD via
219 different coupling types (linear-substituted, *ortho*-substituted or quater-substituted),
220 the exact chemical structure of the obtained product cannot be confirmed at the
221 present stage. However, considering the characterization results and the steric
222 hindrance effects, we assumed that the obtained MON-4COOH was probably the
223 mixture of linear- and *ortho*-substituted polymers.

224 *3.2. Adsorption kinetics*

225 Three initial concentrations (25, 50 and 100 mg L^{-1}) were selected to evaluate the
226 adsorption kinetics of three typical cationic dyes MG, MB and CV on MON-4COOH
227 (Fig. 3; Fig. S6-S10). The MON-4COOH showed fast adsorption kinetics for the
228 studied cationic dyes. When the initial concentration of each dye was 25 mg L^{-1}, the
229 completely adsorption and removal were achieved within 10 seconds for MG and CV,
230 as well as 20 seconds for MB (Fig. 3a-c). In addition, even at a high concentration of
231 100 mg L^{-1}, the adsorption equilibrium for all the studied cationic dyes was achieved
232 and all the cationic dyes were fully removed within 3 min (Fig. 4; Fig. S6-S8),
233 revealing the fast adsorption kinetics of MON-4COOH for cationic dyes. The
234 adsorption capacity of these cationic dyes increased when their concentration

increased (Table 1), indicating the adsorption binding sites on MON-4COOH was sufficient for these cationic dyes and did not reach the saturation at these concentrations range [38]. The adsorption kinetics of the studied cationic dyes on MON-4COOH were faster than the previous reported adsorbents such as metal-organic frameworks, metallic oxides and carbon nanotubes *et al* [17-20], revealing the promise of MON-4COOH for fast removal of cationic dyes from water samples.

To show the selectivity of the designed MON-4COOH for cationic dyes, an anionic dye methyl orange (MO) was chose for comparison (Fig. 3d). MON-4COOH showed much slower kinetic for the adsorption of anionic dye MO (Fig. 3d; Fig. S9) than cationic dyes MG, MB and CV, 3 min were needed to achieve the adsorption equilibrium for MO at 25 mg L^{-1}. However, when the initial concentration of MO was 100 mg L^{-1}, an adsorption capacity of 155.5 mg g^{-1} was obtained on MON-4COOH (Fig. 4d), which also suggested the capability of MON-4COOH for the adsorption and elimination of anionic dye. The adsorption of the studied four organic dyes on MON-4COOH all fitted well with the pseudo-second-order kinetic model (Table 1; Table S2, Fig. S10).

3.3. Adsorption isotherms

Four temperatures at 25-55 ^{o}C were selected to study the adsorption isotherms of these four organic dyes on MON-4COOH (Fig. 5). The adsorption capacity for MB, MG and CV was constantly increased as the initial concentration and temperature increased, revealing higher concentration was favorable for their adsorption and the

adsorption process of these cationic dyes on MON-4COOH was endothermic [35]. The adsorption of these cationic dyes on MON-4COOH followed well with the Langmuir adsorption model, suggesting the monolayer adsorption procedure of MON-4COOH for cationic dyes (Fig. S11) [37]. The maximum adsorption capacity for MG, MB and CV was calculated to be 3126, 2564 and 1114 mg g^{-1}, respectively (Tables S3-5), which was much higher than many other reported adsorbents like ZIF-8, metallic oxides and carbon nanotubes (Tables S6-8) and comparable to the maximum adsorption record of polydopamine nanoparticles (2896 mg g^{-1} for MB) [16] and ZIF-8@GO (3300 mg g^{-1} for MG) [17]. The maximum adsorption capacity of MON-4COOH for MG, MB and CV followed the order of MG > MB > CV. The molecular size of MG, MB and CV were 1.38 × 0.99 × 0.42, 1.26 × 0.77 × 0.65 and 1.41 × 1.21 × 0.18 nm, respectively [24,26,42]. MG with larger molecular size than MB was preferred to adsorb on MON-4COOH. The results may be ascribed to the unique micropores of MON-4COOH at ~1.4 nm, larger MG could enter and bind closer to the micropores, while smaller MB could enter and easily leave the pores. This phenomenon was also observed on previous reported silsesquioxane-based hybrid porous polymers [24,26]. However, CV with the larger or critical molecular size than that of MON-4COOH was unfavorable to enter into the micropores, leading to the lowest adsorption capacity among these three cationic dyes. In contrast, MON-4COOH only gave a maximum adsorption capacity of 455 mg g^{-1} for ionic dye MO (Table S9), which was lower than the cationic dyes, showing the good selectivity of MON-4COOH for cationic dyes. The adsorption capacity of MO on MON-4COOH

was much lower than other adsorbents such as Ni-Co-S/SDS and FH-CoAl (Table S10). In addition, the adsorption process of MO on MON-4COOH was exothermic.

3.4. pH and ionic strength effects

The MON-4COOH also gave good adsorption stability for the studied organic dyes in the pH range of 3-10 and the NaCl concentration below 50 mg L^{-1} (Fig. S12-S13). The results showed that small amount of NaOH or HCl gave little effect on the adsorption capacity of these organic dyes on MON-4COOH in this study. The MG, MB and CV mainly existed as undissociated or positively charged form at neutral or weakly basic conditions (Fig. S14), which were possibly for the formation of hydrogen bonding interaction or electrostatic attraction between cationic dyes and anionic MON-4COOH (Fig. S1). In contrast, the MO existed as negative charged at pH 4-10 (Fig. S14). The electrostatic repulsion between negatively charged MO and MON-4COOH should be a reason for the lower adsorption capacity of MON-4COOH for MO than the studied cationic dyes. The constant adsorption of these dyes on MON-4COOH also revealed hydrogen bonding interaction or electrostatic attraction was not the sole adsorption mechanism on MON-4COOH.

3.5. Flow-through water treatment, desorption, and reusability

The fast kinetic, large adsorption capacity and good adsorption stability prompt us to evaluate the flow-through water treatment ability of MON-4COOH for these four organic dye solutions (Fig. 6). A 50 mg dosage of MON-4COOH was loaded in a solid phase extraction column. The organic dye solution (25 mg L^{-1}) was continuously passed through the MON-4COOH column at a flow rate of 2.0 mL min^{-1} via a flow

injection pump. MON-4COOH gave good flow-through water treatment ability for MG (Fig. 6). The concentration of MG in the eluate was very low even after treating 900 mL of MG (Fig. S15), underling the potential of MON-4COOH for the treatment of MG polluted water. The flow-through water treatment volumes of MON-4COOH for MB, CV and MO were 500, 300 and 100 mL, respectively.

The acetonitrile gave good desorption performance for MG from MON-4COOH (Fig. S16a). Most adsorbed MG was desorbed after three desorption cycles (Fig. S16b). There was no obvious decrease of the adsorption capacity for MG on regenerated MON-4COOH even after five reuse cycles (Fig. S17), indicating the good reusability of MON-4COOH for the studied organic dyes. As there are many conjugated aromatic benzene rings in MG structure, the organic solvent acetonitrile gave good desorption performance for MG from MON-4COOH. The good desorption of MG from MIL-100(Fe), PVP@CNTs-Cu_2O and MOF-hybrid composite was also achieved with acetonitrile and other organic solvents such as methanol and ethanol [10,17,43]. In addition, the regenerated MON-4COOH presented the similar morphology, ^{13}C NMR, BET surface area, and water contact angle to the fresh MON-4COOH (Fig. S18), suggesting MON-4COOH possessed good stability during adsorption.

3.6. Adsorption mechanisms

The possible adsorption mechanisms of MON-4COOH for these organic dyes were firstly elucidated by comparing the adsorption capacity of these dyes on MON, MON-COOH, MON-2COOH and MON-NAP (Fig. 7). The MON without

naphthalene and carboxyl groups showed lower adsorption capacity than other four adsorbents for the studied dyes, suggesting the key roles of naphthalene and carboxyl groups during the dye adsorption in this study. However, the MON still gave the adsorption capacity of 292, 661, 406, and 177 mg g^{-1} for MB, MG, CV and MO, respectively, showing the important roles of hydrophobic and π-π interaction between aromatic MON and organic dyes. The MON-NAP with naphthalene groups gave higher adsorption capacity than MON, further revealing the enhanced π-π and hydrophobic interactions of MON-NAP for organic dyes. The MON-COOH and MON-2COOH with carboxyl groups gave higher adsorption capacity than MON, confirming the significant roles of electrostatic attraction or hydrogen bonding interaction resulted from the carboxyl groups during the adsorption process. In addition, MON-4COOH with both naphthalene and carboxyl groups gave the largest adsorption capacities than other four adsorbents, proving the key roles of electrostatic attraction, hydrophobic and π-π interactions resulted from the incorporated naphthalene and carboxyl groups for the rapid adsorption and efficient removal of organic dyes from water. The much higher adsorption capacity of MON-4COOH for MG than MB and CV resulted from the differences of cationic dyes' molecular sizes [26] and the better adsorption of MON-4COOH for MG than MB and CV at a high initial concentration of 2 mg mL^{-1}.

The hypothesis of electrostatic attraction between MON-4COOH and cationic dyes was elucidated in section 3.4. To further reveal the better selectivity of MON-4COOH for cationic dyes than anionic dyes, the adsorption of additional two

anionic dyes AB75 and AR on MON-4COOH was compared (Fig. S19). The adsorption capacity of cationic dyes (MB, MG and CV) was quite higher than anionic dyes (MO, AR and AB75) on MON-4COOH, highlighting the good selectivity of MON-4COOH for cationic dyes.

The MON-4COOH before and after MG adsorption was further studied by XPS experiments to elucidate the possible binding sites on MON-4COOH during the adsorption (Fig. 8). The O1s peaks at 529.405 and 531.007 eV were assigned to the C=O and -OH groups on MON-4COOH, confirming the successful hydrolysis of DBTD to form -COOH groups on MON-4COOH [44-48]. These O1s peaks were shifted to 529.392 and 530.912 eV after the adsorption of MG, respectively, suggesting the proper interaction sites of -COOH groups to MG [44]. The C1s peaks at 288.762, 285.584 and 284.599 eV were assigned to the C signals of O=C-OH, aromatic and benzene groups on MON-4COOH, respectively [10,37,48]. The shifting of O=C-OH from 288.762 to 288.540 eV after MG adsorption also suggested the electrostatic attraction of MON-4COOH and MG [44]. In addition, the aromatic and benzene C1s peaks at 284.599 and 285.584 eV were moved to 284.578 and 285.397 eV after the adsorption of MG, respectively, showing the proper π-π or hydrophobic interaction between aromatic MON-4COOH and MG [10,37]. These results suggested the important roles of electrostatic attraction, hydrophobic and π-π interaction between cationic dyes and MON-4COOH in the adsorption process.

4. Conclusions

In summary, we have reported a convenient and facile anhydride hydrolysis

strategy to synthesize a novel dual-functionalized MON-4COOH with enriched naphthalene and carboxyl groups for efficient removal of cationic dyes from water. The multiple and abundant interaction sites within MON-4COOH's networks led to the fast kinetic and remarkable adsorption capacity for cationic dyes. The good flow-through water treatment ability also made MON-4COOH highly potential for the remediation of cationic dyes polluted water. This work provides a feasible way to design and synthesize functionalized MONs for efficient removal and elimination of environmental pollutants.

Declarations of interest

There are no conflicts to declare.

Acknowledgements

This work was supported by the National Key Research and Development Program of China (2018YFC1602401), the National Natural Science Foundation of China (21777074), the Tianjin Natural Science Foundation (18JCQNJC05700), and the Fundamental Research Funds for the Central Universities.

Appendix A. Supplementary data

Supplementary data to this article can be found online at https://.

References

[1] X.J. Zhang, C. Chen, P.F. Lin, A.X. Hou, Z.B. Niu, J. Wang, Emergency drinking water treatment during source water pollution accidents in China:

origin analysis, framework and technologies, Environ. Sci. Technol. 45 (2011) 161-167.

[2] M. Soldatov, H.Z. Liu, A POSS-phosphazene based porous material for adsorption of metal ions from water, Chem. Asian J. 14 (2019) 4345-4351.

[3] A. Chowdhury, A.A. Khan, S. Kumari, S. Hussain, Superadsorbent Ni-Co-S/SDS nanocomposites for ultrahigh removal of cationic, anionic organic dyes and toxic metal ions: kinetics, isotherm and adsorption mechanism, ACS Sustainable Chem. Eng. 7 (2019) 4165-4176.

[4] E. Forgacs, T. Cserhati, G. Oros, Removal of synthetic dyes from wastewaters: a review, Environ. Int. 30 (2004) 953-971.

[5] P.V. Nidheesh, M.H. Zhou, M.A. Oturan, An overview on the removal of synthetic dyes from water by electrochemical advanced oxidation processes, Chemosphere 197 (2018) 210-227.

[6] G. Crini, Non-conventional low-cost adsorbents for dye removal: A review, Bioresource Technol. 97 (2006) 1061-1085.

[7] G. Crini, P.M. Badot, Application of chitosan, a natural aminopolysaccharide, for dye removal from aqueous solutions by adsorption processes using batch studies: A review of recent literature, Prog. Polym. Sci. 33 (2008) 399-447.

[8] M.T. Yagub, T.K. Sen, S. Afroze, H.M. Ang, Dye and its removal from aqueous solution by adsorption: A review, Adv. Colloid Interface Sci. 209 (2014) 172-184.

[9] A. Demirbas, Agricultural based activated carbons for the removal of dyes from aqueous solutions: A review, J. Hazard. Mater. 167 (2009) 1-9.

[10]X. Li, Y. Zhang, L. Jing, X. He, Novel N-doped CNTs stabilized Cu_2O nanoparticles as adsorbent for enhancing removal of Malachite Green and tetrabromobisphenol A, Chem. Eng. J. 292 (2016) 326-339.

[11]V.K. Gupta, R. Kumar, A. Nayak, T.A. Saleh, M.A. Barakat, Adsorptive removal of dyes from aqueous solution onto carbon nanotubes: A review, Adv. Colloid Interface Sci. 193 (2013) 24-34.

[12]H. Gao, R. Cao, X. Xu, J. Xue, S. Zhang, T. Hayat, N.S. Alharbi, J. Li, Surface area- and structure-dependent effects of LDH for highly efficient dye removal, ACS Sustainable Chem. Eng. 7 (2019) 905-915.

[13]M. Zhou, T. Wang, Z. He, Y. Xu, W. Yu, B. Shi, K. Huang, Synthesis of yolk-shell magnetic porous organic nanospheres for efficient removal of methylene blue from water, ACS Sustainable Chem. Eng. 7 (2019) 2924-2932.

[14]L. Zhang, H. Lu, J. Yu, E. Mcsporran, A. Khan, Y. Fan, Y. Yang, Z. Wang, Y. Ni, Preparation of high-strength sustainable lignocellulose gels and their applications for antiultraviolet weathering and dye removal, ACS Sustainable Chem. Eng. 7 (2019) 2998-3009.

[15]T. Huang, M. Yan, K. He, Z. Huang, G. Zeng, A. Chen, M. Peng, H. Li, L. Yuan, G. Chen, Efficient removal of methylene blue from aqueous solutions using magnetic graphene oxide modified zeolite, J. Colloid Interface Sci. 543 (2019) 43-51.

[16]J.Y. Lin, H.B. Wang, E.H. Ren, Q.S. Song, J.W. Lan, S. Chen, B. Yan, Stomatocyte-like hollow polydopamine nanoparticles for rapid removal of water-soluble dyes from water, Chem. Commun. 55 (2019) 8162-8165.

[17]J. Abdi, M. Vossoughi, N.M. Mahmoodi, I. Alemzadeh, Synthesis of metal-organic framework hybrid nanocomposites based on GO and CNT with high adsorption capacity for dye removal, Chem. Eng. J. 326 (2017) 1145-1158.

[18]M. Sarker, S. Shin, J.H. Jeong, S.H. Jhung, Mesoporous metal-organic framework PCN-222(Fe): Promising adsorbent for removal of big anionic and cationic dyes from water, Chem. Eng. J. 371 (2019) 252-259.

[19]Q. Zhang, J. Yu, J. Cai, R. Song, Y. Cui, Y. Yang, B. Chen, G. Qian, A porous metal-organic framework with -COOH groups for highly efficient pollutant removal, Chem. Commun. 50 (2014) 14455-14458.

[20]X. Liu, Z. Xiao, J. Xu, W. Xu, P. Sang, L. Zhao, H. Zhu, D. Sun, W. Guo, A NbO-type copper metal-organic framework decorated with carboxylate groups exhibiting highly selective CO_2 adsorption and separation of organic dyes, J. Mater. Chem. A 4 (2016) 13844-13851.

[21]S. Karak, K. Dey, A. Torris, A. Halder, S. Bera, F. Kanheerampockil, R. Banerjee, Inducing disorder in order: hierarchically porous covalent organic framework nanostructures for rapid removal of persistent organic pollutants, J. Am. Chem. Soc. 141 (2019) 7572-7581.

[22]G.B. Kunde, B. Sehgal, A.G. Ganguli, Synthesis of mesoporous rebar MWCNT/alumina composite (RMAC) nodules for the effective removal of methylene blue and Cr (VI) from an aqueous medium, J. Hazard. Mater. 374 (2019) 140-151.

[23]W.L. Li, C.D. Jiang, H.H. Liu, Y.H. Yan, H.Z. Liu, Octa[4-(9-carbazolyl)phenyl]silsesquioxane-based porous material for dyes adsorption and sensing of nitroaromatic compounds, Chem. Asian J. 14 (2019) 3363-3369.

[24]M.T. Ge, H.Z. Liu, A silsesquioxane-based thiophene-bridged hybrid nanoporous network as a highly efficient adsorbent for wastewater treatment, J. Mater. Chem. A 4 (2016) 16714-16722.

[25]H.H. Liu, H.Z. Liu, Selective dye adsorption and metal ion detection using multifunctional silsesquioxane-based tetraphenylethene-linked nanoporous polymers, J. Mater. Chem. A 5 (2017) 9156-9162.

[26]X.R. Yang, H.Z. Liu, Diphenylphosphine-substituted ferrocene/silsesquioxane-based hybrid porous polymers as highly efficient adsorbents for water treatment, ACS Appl. Mater. Interfaces 11 (2019) 26474-26482.

[27]J.X. Jiang, F.B. Su, A. Trewin, C.D. Wood, H.J. Niu, J.T.A. Jones, Y.Z. Khimyak, A.I. Cooper, Synthetic control of the pore dimension and surface area in conjugated microporous polymer and copolymer networks, J. Am. Chem. Soc. 130 (2008) 7710-7720.

[28]J. Jiang, F. Su, A. Trewin, C.D. Wood, N.L. Campbell, H. Niu, C. Dickinson, A.Y. Ganin, M.J. Rosseinsky, Y.Z. Khimyak, A.I. Cooper, Conjugated microporous poly(aryleneethynylene) networks, Angew. Chem. Int. Ed. 46 (2007) 8574-8578.

[29]N. Kang, J.H. Park, M. Jin, N. Park, S.M. Lee, H.J. Kim, J.M. Kim, S.U. Son, Microporous organic network hollow spheres: useful templates for nanoparticulate Co_3O_4 hollow oxidation catalysts, J. Am. Chem. Soc. 135 (2013) 19115-19118.

[30]W.K. Meng, L. Liu, X. Wang, R.S. Zhao, M.L. Wang, J.M. Lin, Polyphenylene core-conjugated microporous polymer coating for highly sensitive solid-phase microextraction of polar phenol compounds in water samples, Anal. Chim. Acta 1015 (2018) 27-34.

[31]S. Hong, J. Yoo, N. Park, S.M. Lee, J. Park, J.H. Park, S.U. Son, Hollow Co@C prepared from a Co-ZIF@microporous organic network: magnetic adsorbents for aromatic pollutants in water, Chem. Commun. 51 (2015) 17724-17727.

[32]J. Chun, S. Kang, N. Park, E.J. Park, X. Jin, K.D. Kim, H.O. Seo, S.M. Lee, H.J. Kim, W.H. Kwon, Y.K. Park, J.M. Kim, Metal-organic framework@microporous organic network: hydrophobic adsorbents with a crystalline innerporosity, J. Am. Chem. Soc. 136 (2014) 6786-6789.

494 [33]J. Li, H. Li, Y. Zhao, S. Wang, X. Chen, R.S. Zhao, A hollow microporous
495 organic network as a fiber coating for solid-phase microextraction of
496 short-chain chlorinated hydrocarbons, Microchimica Acta 185 (2018) 416.
497 [34]B. Liang, H. Wang, X. Shi, B. Shen, X. He, Z.A. Ghazi, N.A. Khan, H. Sin,
498 A.M. Khattak, L. Li, Z. Tang, Microporous membranes comprising conjugated
499 polymers with rigid backbones enable ultrafast organic-solvent nanofiltration,
500 Nat. Chem. 10 (2018) 961-967.
501 [35]Y.Y. Cui, H.B. Ren, C.X. Yang, X.P. Yan, Room-temperature synthesis of
502 microporous organic network for efficient adsorption and removal of
503 tetrabromobisphenol A from aqueous solution, Chem. Eng. J. 368 (2019)
504 589-597.
505 [36]Y. Liu, Y. Cui, C. Zhang, J. Du, S. Wang, Y. Bai, Z. Liang, X. Song,
506 Post-cationic modification of a pyrimidine□based conjugated microporous
507 polymer for enhancing the removal performance of anionic dyes in water,
508 Chem. Eur. J. 24 (2018) 7480-7488.
509 [37]Y.Y. Cui, H.B. Ren, C.X. Yang, X.P. Yan, Facile synthesis of hydroxyl
510 enriched microporous organic networks for enhanced adsorption and removal
511 of tetrabromobisphenol A from aqueous solution, Chem. Eng. J. 373 (2019)
512 606-615.
513 [38]Z.D. Du, Y.Y. Cui, C.X. Yang, X.P. Yan, Core-shell magnetic
514 amino-functionalized microporous organic network nanospheres for the

515 removal of tetrabromobisphenol A from aqueous solution, ACS Appl. Nano
516 Mater. 2 (2019) 1232-1241.
517 [39]S.A. Ali, I.Y. Yaagoob, M.A.J. Mazumder, H.A. Al-Muallem, Fast removal of
518 methylene blue and Hg(II) from aqueous solution using a novel
519 super-adsorbent containing residues of glycine and maleic acid, J. Hazard.
520 Mater. 369 (2019) 642-654.
521 [40]M.M. Zhang, H.C. Yu, B.B. Chen, Facile synthesis of EDTA-functionalized
522 halloysite nanotubes for the removal of methylene blue from aqueous phase,
523 Can. J. Chem. 97 (2019) 259-266.
524 [41]A.C.S. Talari, Z. Movasaghi, S. Rehman, I. Rehman, Raman spectroscopy of
525 biological tissues, Appl. Spectrosc. Rev. 50 (2015) 46-111.
526 [42]S.H. Huo, X.P. Yan, Metal-organic framework MIL-100(Fe) for the
527 adsorption of malachite green from aqueous solution, J. Mater. Chem. 22
528 (2012) 7449-7455.
529 [43]S.H. Huo, C.X. Liu, P.X. Zhou, J. Yu, L. Bai, Z.G. Han, X.Q. Lu, Recyclable
530 magnetic carbonaceous porous composites derived from MIL-100(Fe) for
531 superior adsorption and removal of malachite green from aqueous solution,
532 RSC Adv. 9 (2019) 23711-23717.
533 [44]P. Zhang, D.Y. Hou, D. O'Connor, X.R. Li, S. Pehkonen, R.S. Varma, X.
534 Wang, Green and size-specific synthesis of stable Fe-Cu oxides as
535 earth-abundant adsorbents for malachite green removal, ACS Sustainable
536 Chem. Eng. 6 (2018) 9229-9236.

[45]C.X. Gui, Q.Q. Wang, S.M. Hao, J. Qu, P.P. Huang, C.Y. Cao, W.G. Song, Z.Z. Yu, Sandwichlike magnesium silicate/reduced graphene oxide nanocomposite for enhanced Pb^{2+} and methylene blue adsorption, ACS Appl. Mater. Interfaces 6 (2014) 14653-14659.

[46]J. Qu, Y.X. Yin, Y.Q. Wang, Y. Yan, Y.G. Guo, W.G. Song, Layer structured α□Fe_2O_3 nanodisk/reduced graphene oxide composites as high-performance anode materials for lithium-ion batteries, ACS Appl. Mater. Interfaces 5 (2013) 3932-3936.

[47]G.M. Zhou, D.W. Wang, L.C. Yin, N. Li, F. Li, H.M. Cheng, Oxygen bridges between NiO nanosheets and graphene for improvement of lithium storage, ACS Nano 6 (2012) 3214-3223.

[48]M.C. Hsiao, C.M. Ma, J.C. Chiang, K.K. Ho, T.Y. Chou, X.F. Xie, C.H. Tsai, L.H. Chang, C.K. Hsieh, Thermally conductive and electrically insulating epoxy nanocomposites with thermally reduced grapheme oxide-silica hybrid nanosheets, Nanoscale 5 (2013) 5863-5871.

552 **Figure Captions**

553 **Fig. 1.** Schematic illustration for the synthesis of MON-4COOH and its possible
554 adsorption mechanisms for MG.

555 **Fig. 2.** (a) Solid ^{13}C NMR spectrum, (b) FT-IR spectra, (c) N_2 adsorption-desorption
556 isotherms, (d) TGA curve, (e) FE-SEM image and (f) water contact angle of the
557 synthesized MON-4COOH.

558 **Fig. 3.** UV spectra of (a) MG, (b) MB, (c) CV and (d) MO for different contact time
559 on MON-4COOH. The insets show the filtrates of each dye (25 mg L^{-1}) before and
560 after adsorption on MON-4COOH.

561 **Fig. 4.** Time-dependent adsorption of (a) MG, (b) MB, (c) CV and (d) MO on
562 MON-4COOH at di□erent initial concentrations.

563 **Fig. 5.** Adsorption isotherms of (a) MG, (b) MB, (c) CV and (d) MO on
564 MON-4COOH at di□erent temperatures.

565 **Fig. 6.** Flow-through water treatment pictures of MON-4COOH for MG (25 mg L^{-1}).

566 **Fig. 7.** Comparison of the adsorption capacity on diverse MON sorbents.

567 **Fig. 8.** The XPS spectra of MON-4COOH before (a, b) and after (c, d) MG
568 adsorption.

Table 1 Pseudo-second-order kinetic parameters for the adsorption of MG, MB and CV on MON-4COOH.

Dyes	C_0 (mg L^{-1})	Parameters			
		K_2 (g mg^{-1} s^{-1})	$q_{e,cal}$ (mg g^{-1})	$q_{e,\ exp}$ (mg g^{-1})	R^2
MG	25	-	50.0	50.0	0.999
	50	9.8×10^{-3}	101.4	100.0	0.999
	100	8.3×10^{-4}	203.4	200.0	0.998
MB	25	4.0×10^{-2}	50.2	50.0	0.999
	50	1.8×10^{-2}	100.4	100.0	0.999
	100	1.2×10^{-3}	203.6	200.0	0.999
CV	25	-	50.0	50.0	0.999
	50	3.2×10^{-2}	100.2	100.0	0.999
	100	3.2×10^{-4}	204.3	200.0	0.998

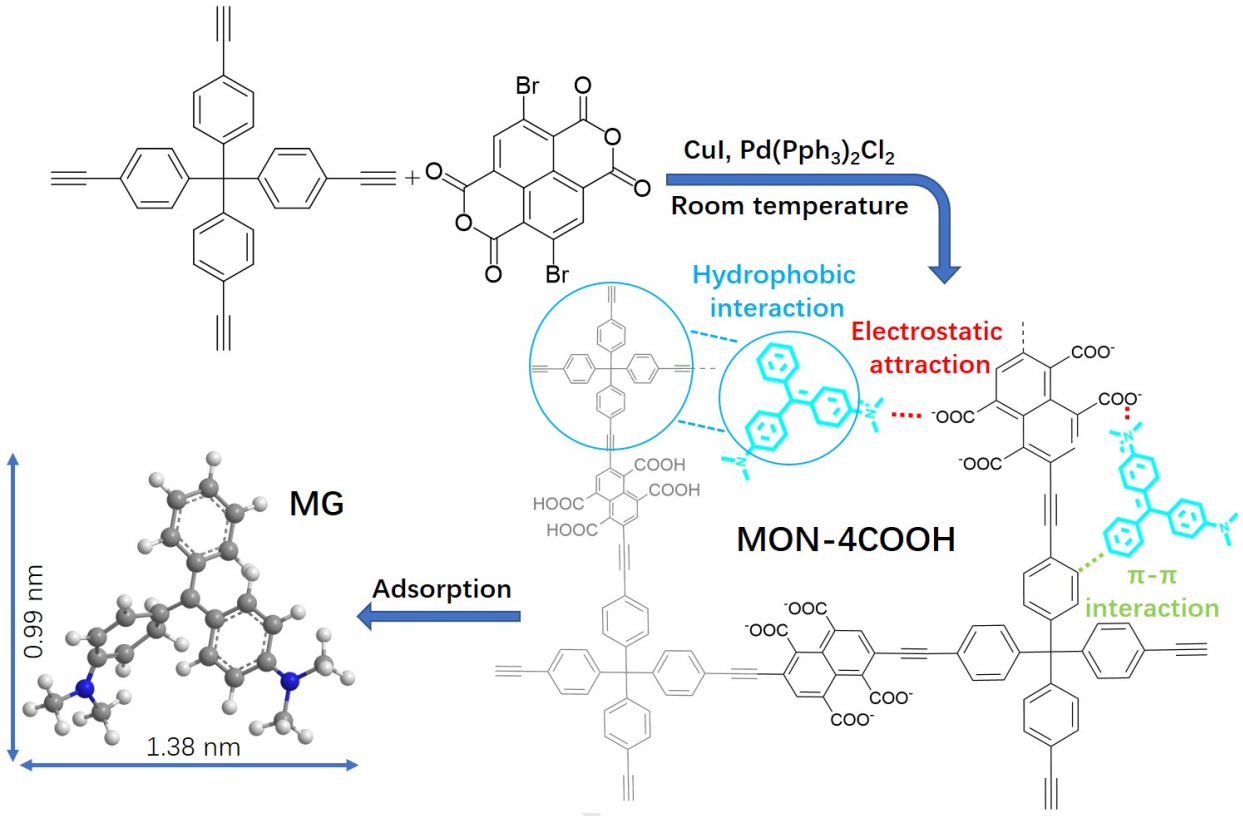

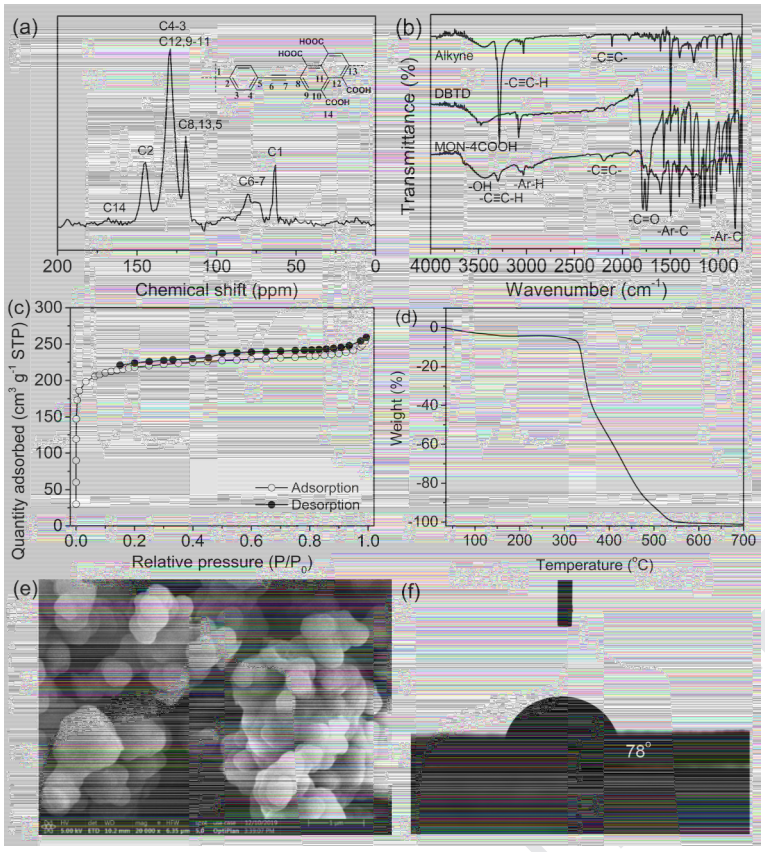

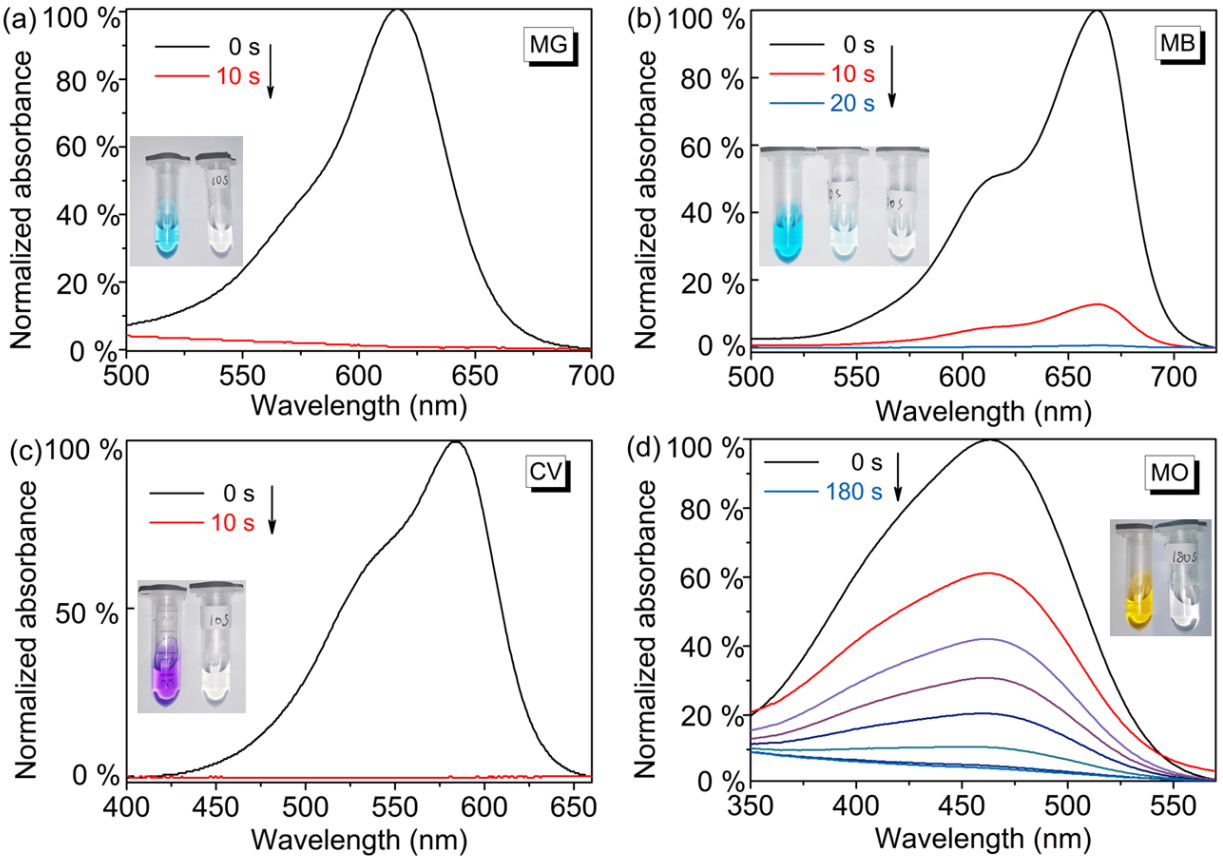
(a)
MG
0 s
10 s
Normalized absorbance
Wavelength (nm)
(b)
MB
0 s
10 s
20 s
Normalized absorbance
Wavelength (nm)
(c)
CV
0 s
10 s
Normalized absorbance
Wavelength (nm)
(d)
MO
0 s
180 s
Normalized absorbance
Wavelength (nm)

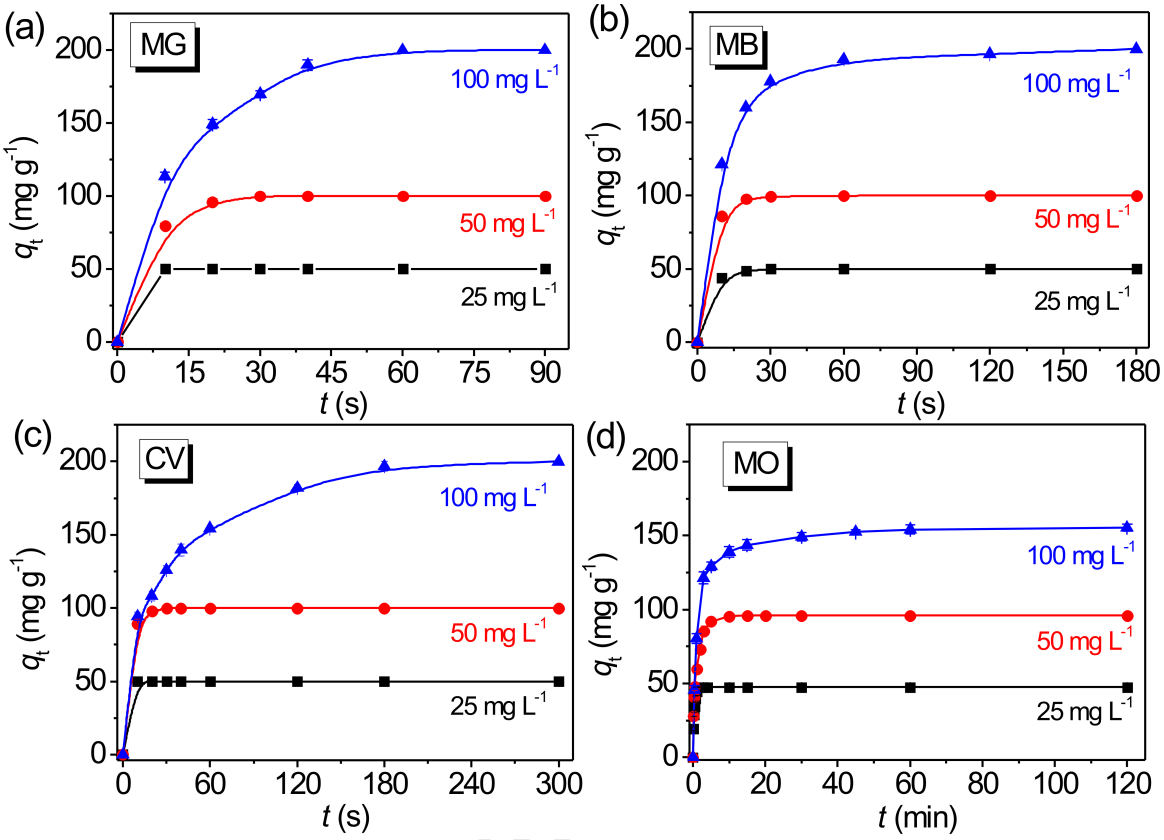
(a)
MG
100 mg L-1
50 mg L-1
25 mg L-1
qt (mg g-1)
t (s)
(b)
MB
100 mg L-1
50 mg L-1
25 mg L-1
qt (mg g-1)
t (s)
(c)
CV
100 mg L-1
50 mg L-1
25 mg L-1
qt (mg g-1)
t (s)
(d)
MO
100 mg L-1
50 mg L-1
25 mg L-1
qt (mg g-1)
t (min)

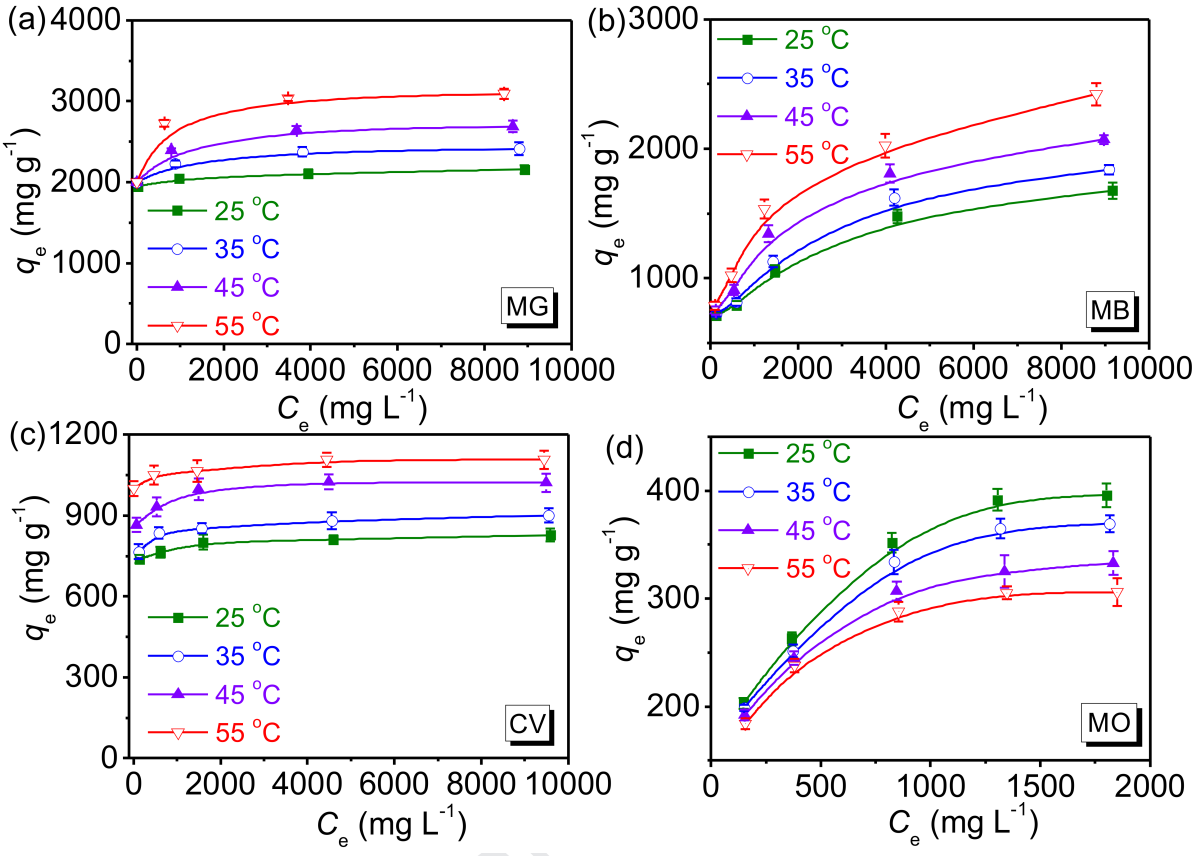

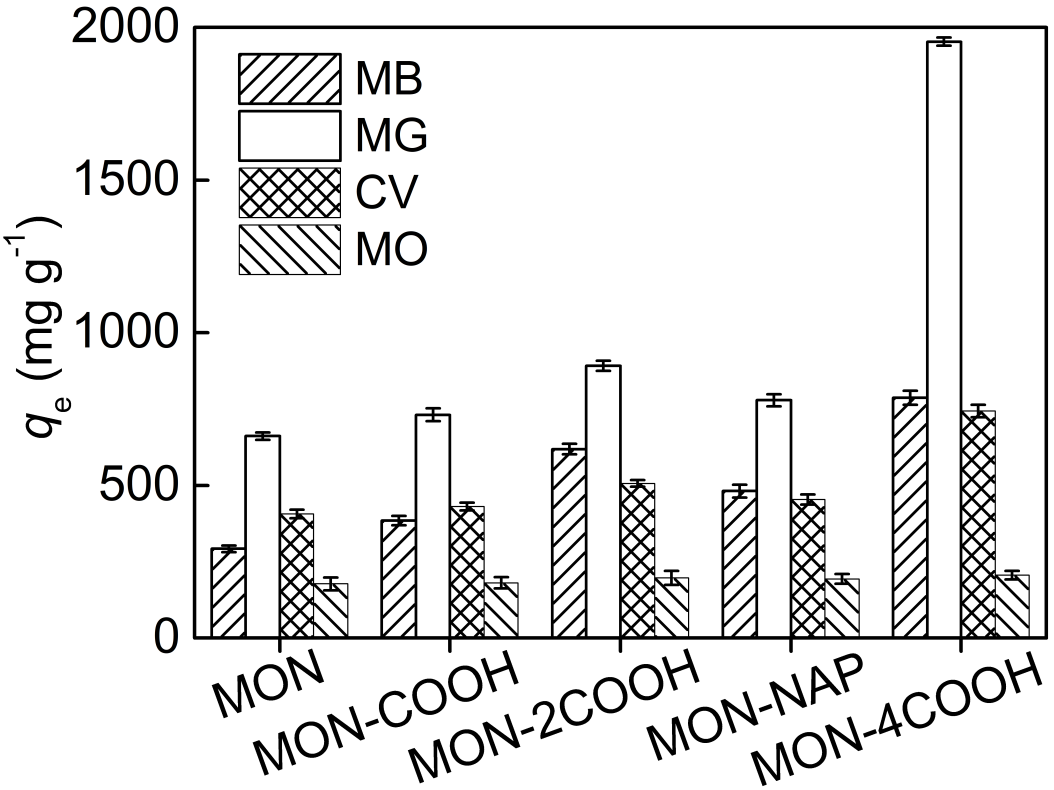
2000
1500
1000
500
0
q_e (mg g^{-1})
MB
MG
CV
MO
MON
MON-COOH
MON-2COOH
MON-NAP
MON-4COOH

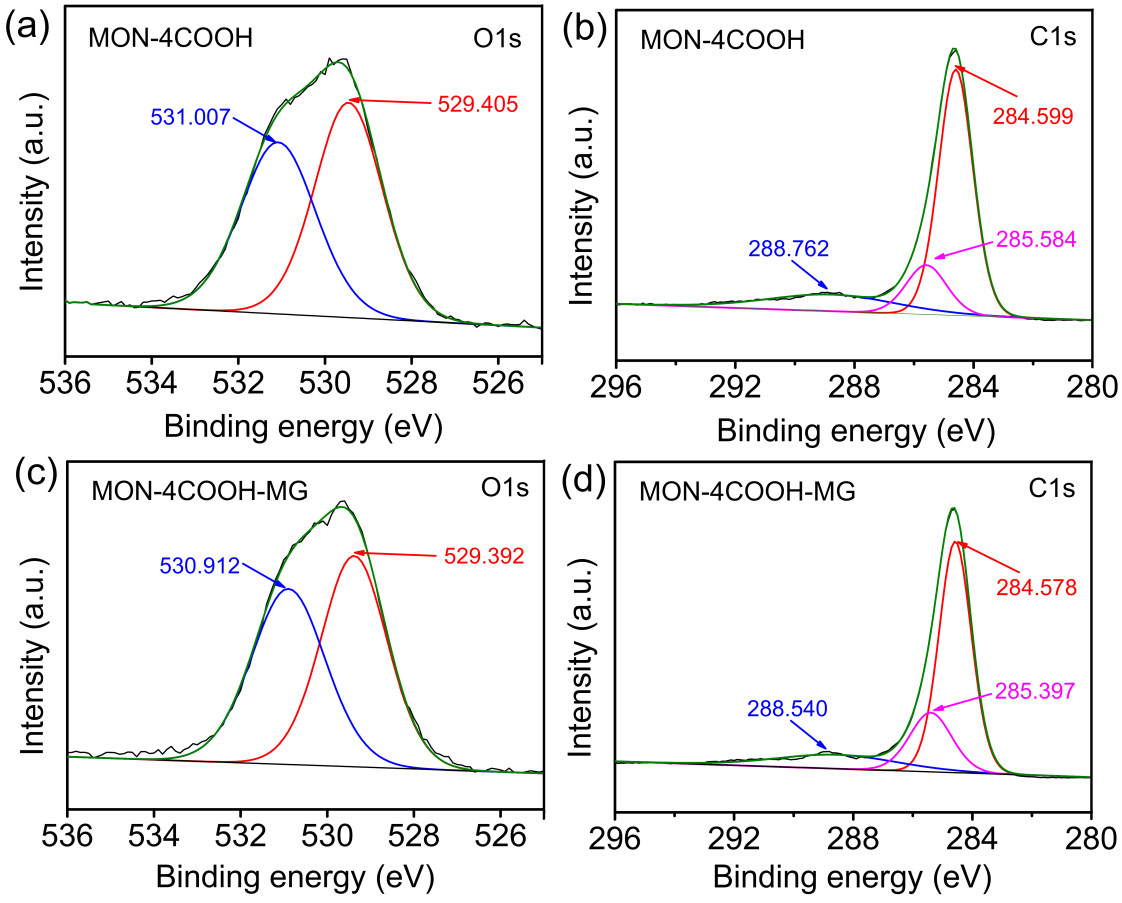
(a)
MON-4COOH
O1s
531.007
529.405
Intensity (a.u.)
536 534 532 530 528 526
Binding energy (eV)
(b)
MON-4COOH
C1s
284.599
288.762
285.584
Intensity (a.u.)
296 292 288 284 280
Binding energy (eV)
(c)
MON-4COOH-MG
O1s
530.912
529.392
Intensity (a.u.)
536 534 532 530 528 526
Binding energy (eV)
(d)
MON-4COOH-MG
C1s
284.578
288.540
285.397
Intensity (a.u.)
296 292 288 284 280
Binding energy (eV)

Highlights

- MON-4COOH was facile synthesized for efficient removal of cationic dyes.
- Completely adsorption of cationic dyes (25 mg L^{-1}) was achieved within 20 seconds.
- MON-4COOH gave q_{max} of 3126, 2564 and 1114 mg g^{-1} for MG, MB and CV, respectively.

CRediT authorship contribution statement

Li Xue: Conceptualization, Methodology, Investigation, Writing - Original Draft **Cui Yuan-Yuan:** Investigation **Chen Ying-Jun:** Validation **Yang Cheng-Xiong:** Conceptualization, Resources, Funding acquisition, Supervision, Project administration, Writing - Review & Editing **Yan Xiu-Ping:** Supervision.

Declaration of Interest Statement

The authors declare that they have no known competing financial interests or personal relationships that could have appeared to influence the work reported in this paper.